Optimizing Conical Intersections without Derivative Coupling Vectors: Application to Multistate Multireference Second-Order Perturbation Theory (MS-CASPT2) †

ARTICLE *in* THE JOURNAL OF PHYSICAL CHEMISTRY B · FEBRUARY 2008

Impact Factor: 3.3 · DOI: 10.1021/jp0761618 · Source: PubMed

3 AUTHORS, INCLUDING:

Joshua D Coe
Los Alamos National Laboratory
30 PUBLICATIONS **482** CITATIONS
SEE PROFILE

Todd J. Martinez
Stanford University
239 PUBLICATIONS **7,875** CITATIONS
SEE PROFILE

Optimizing Conical Intersections without Derivative Coupling Vectors: Application to Multistate Multireference Second-Order Perturbation Theory (MS-CASPT2)†

Benjamin G. Levine, Joshua D. Coe, and Todd J. Martínez*

Department of Chemistry and The Beckman Institute, University of Illinois, Urbana, Illinois 61801

Received: August 1, 2007; In Final Form: October 28, 2007

We introduce a new method for optimizing minimal energy conical intersections (MECIs), based on a sequential penalty constrained optimization in conjunction with a smoothing function. The method is applied to optimize MECI geometries using the multistate formulation of second-order multireference perturbation theory (MS-CASPT2). Resulting geometries and energetics for conjugated molecules including ethylene, butadiene, stilbene, and the green fluorescent protein chromophore are compared with state-averaged complete active space self-consistent field (SA-CASSCF) and, where possible, benchmark multireference single- and double-excitation configuration interaction (MRSDCI) optimizations. Finally, we introduce the idea of "minimal distance conical intersections", which are points on the intersection seam that lie closest to some specified geometry such as the Franck−Condon point or a local minimum on the excited state.

Introduction

Conical intersections (true crossings of two or more adiabatic electronic states) play a key role in the mechanisms of photochemical reactions.[1−8] Examples of such reactions include cis−trans photoisomerization[3,9] and the primary events in vision,[7,10] excited-state proton transfer,[11] and photodamage to DNA.[12] In many cases, it is fruitful to think of intersections as the analogues of transition states for reactions that occur purely on the ground electronic state. However, conical intersections are not isolated points, but rather multidimensional seams. Thus, it is natural to seek a specific molecular geometry along the intersection seam that might dominate nonadiabatic transitions between electronic states. Minimal energy conical intersections (MECIs) have been proposed as just such points, being defined as local minima on the intersection seam. It is now understood that MECIs cannot provide the whole story regarding photochemical mechanisms, and dynamical calculations are required in most cases. This is simply because excited-state lifetimes are often very short, and there is insufficient time for equilibration prior to surface crossing, or, to put it another way, the molecular wavepacket often encounters an intersection which lies at a higher energy than the nearest MECI.[3,13] Nevertheless, MECIs provide a useful set of geometries that can be used to characterize the mechanism; there are usually a number of different MECIs connecting any two electronic states, and these can often be related to the electronic character of the two adiabatic states in the neighborhood of the MECI. For example, one MECI might arise from the intersection of two covalent electronic states, and another might arise from the intersection of a covalent state with a charge transfer state.[9,14−16] Thus, it is useful to locate MECI geometries both in preliminary studies of the excited-state potential energy surface (PES) and also in order to characterize the extent of equilibration on the excited-state in dynamics calculations. For example, the probability of quenching through several different MECIs as determined by a dynamical calculation may not reflect the energetic ordering of the MECIs. In this case, the molecule is not equilibrated on the excited-state and dynamical effects may be considered essential to understand the photochemistry. However, it might also be useful to consider other special points along the intersection

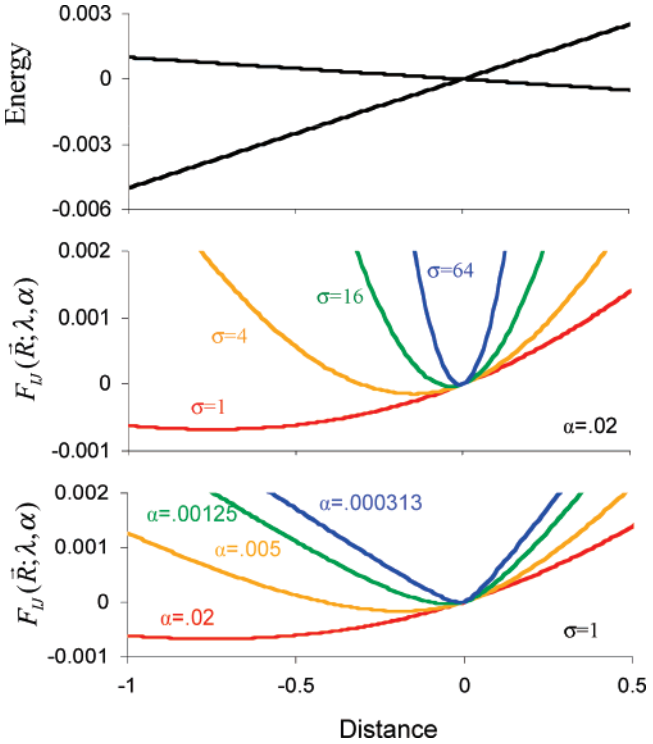

Figure 1. Illustration of convergence of the minimum of F_{IJ} to a conical intersection as α and σ are varied. The top panel shows the energies of the two states of a model PES around a conical intersection. The middle panel shows the behavior of F_{IJ} as σ is varied for constant α. As σ is increased, the minimum of F_{IJ} converges toward the CI. The lower panel shows the behavior of F_{IJ} as the smoothing parameter α is varied for constant σ. As α is decreased, the minimum of F_{IJ} converges to the intersection point, but F_{IJ} also becomes more sharply varying (in the limit that α vanishes, the derivative discontinuity of the underlying adiabatic states appears in F_{IJ}).

† Part of the "James T. (Casey) Hynes Festschrift".

* To whom correspondence should be addressed.

10.1021/jp0761618 CCC: $40.75
Published on Web 12/15/2007

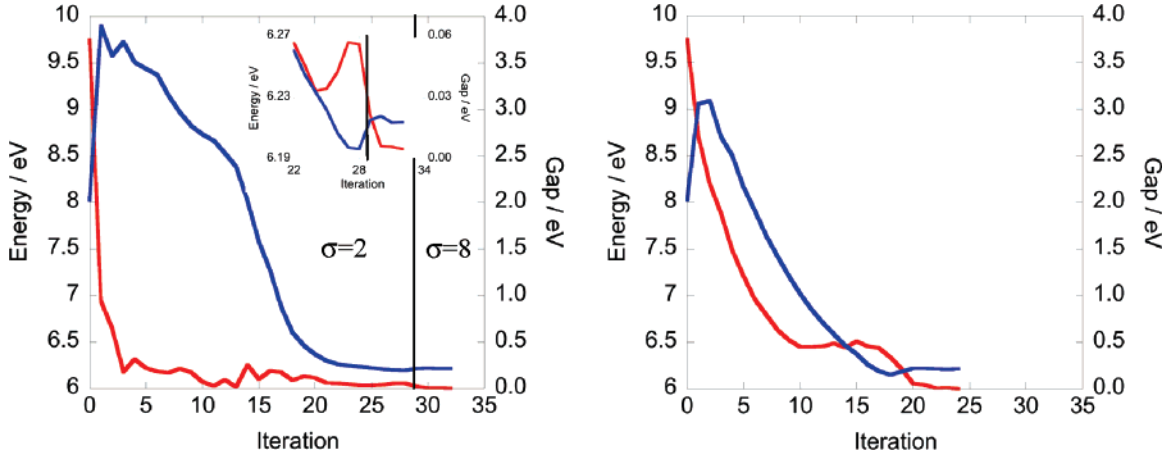

Figure 2. Left panel: Convergence behavior of the excited-state energy (blue) and the energy gap (red) during a typical MECI optimization using the CIOpt algorithm. The CIOpt algorithm locates the intersection seam quickly and then follows the seam until convergence is achieved for the initial value of σ. If the energy gap is larger than a chosen threshold, σ is increased and the optimization continues. The last ten iterations can be seen on an expanded scale in the inset. Right panel: Convergence behavior of an MECI optimization utilizing the Bearpark-Robb-Schlegel algorithm for the same molecule. The number of iterations necessary to converge is only slightly less than the CIOpt algorithm, even though CIOpt does not utilize derivative coupling information.

seam, for example, the intersection that is closest to a particular geometry such as the Franck−Condon point or a local minimum on the excited state. We call these "minimal distance conical intersections" or MDCIs, and introduce them in this work.

Most well-established optimization algorithms assume smoothness of the function to be optimized. Since the PES necessarily has a discontinuous first derivative in the vicinity of a conical intersection, previous algorithms for finding MECIs have required access to the gradient difference and derivative coupling (also known as nonadiabatic coupling) vectors which define the "branching plane". These two molecular displacement vectors define the directions in which derivative discontinuities are required. Several schemes for optimization of MECIs have been developed for cases where energy gradients and derivative couplings are readily available.[17−20] Analytic gradient methodology allows efficient calculation of these gradient and coupling vectors for many electronic structure methods.[21] Currently, many MECI optimizations employ the state-averaged complete active space self-consistent field (SA-CASSCF) method[22] to describe the potential energy surface (PES), largely because this method is both capable of describing multireference character of the wavefunction near an intersection and has the required gradient and coupling vectors available. However, the SA-CASSCF method does not efficiently describe dynamic electron correlation effects, and this can lead to results of uncertain accuracy. Thus, it may be desirable to employ a more accurate description of the PES in conical intersection optimization. Unfortunately, the coding of schemes to evaluate derivative coupling vectors is cumbersome, and thus implementations do not exist for many electronic structure methods. Recently, the required codes have been developed for the multireference single and double excitation configuration interaction (MRSDCI) method,[23,24] but computational cost makes it difficult to apply MRSDCI to molecules with more than 10 atoms. Additionally, there are potentially accurate electronic structure methods for which the electronic wavefunction is not uniquely defined, and therefore, the formalism for computing derivative coupling vectors is not completely developed, e.g., time-dependent density functional theory[25] (TDDFT) and renormalized coupled-cluster theories.[26]

An additional motivation for the present work lies in recent interest in the role of conical intersections for excited-state dynamics in solution and condensed phase environments.[27−35] In complex environments, it may be fruitful to deal with free energy surfaces rather than PESs, in which case one must again face the conceptual issue that the electronic wavefunction is not uniquely defined and, therefore, the formalism for evaluating derivative couplings may not always be clear.

In this paper, we present a new MECI optimization scheme. Our method may be applied to any electronic structure method that associates unique energies with a particular molecular geometry; that is, it requires neither energy gradient nor derivative coupling vectors. An early version of this algorithm has been used to characterize the behavior of TDDFT in regions near intersections.[36] Multireference second-order perturbation theory[37] (CASPT2) provides an efficient and accurate way to add dynamic electron correlation effects to SA-CASSCF. However, derivative coupling vectors are not yet implemented at this level of theory, heretofore posing an obstacle to complete optimization of MECIs with CASPT2.

There are two distinct classes of CASPT2 methods: single state[38] (SS-CASPT2) and multistate[39] (MS-CASPT2). In SS-CASPT2, the energies of the CASSCF eigenvectors are modified by the perturbation, but no further mixing of the perturbed states with each other is allowed. This can lead to artifacts near avoided crossings and conical intersections, as Serrano-Andres et al. have previously shown.[40] In contrast, MS-CASPT2 methods account for the subsequent mixing of the perturbed states through the construction and diagonalization of an effective Hamiltonian matrix. MECI geometries have been previously optimized with SS-CASPT2[40,41] and MS-CASPT2[40] by using approximate derivative coupling vectors. Additionally, it has been noted that MS-CASPT2 may require large active spaces for the proper description of PESs near MECIs.[40] We apply our new method to carry out the first complete optimization of MECIs with the MS-CASPT2 method. For small molecules, the results are compared to MRSDCI in order to assess the accuracy of MECIs determined using MS-CASPT2.

Methods

The two most frequently used methods for the optimization of MECIs between adiabatic electronic states I and J (upper and lower, respectively) are based on Lagrange multiplier techniques, minimizing the energy of the upper electronic state

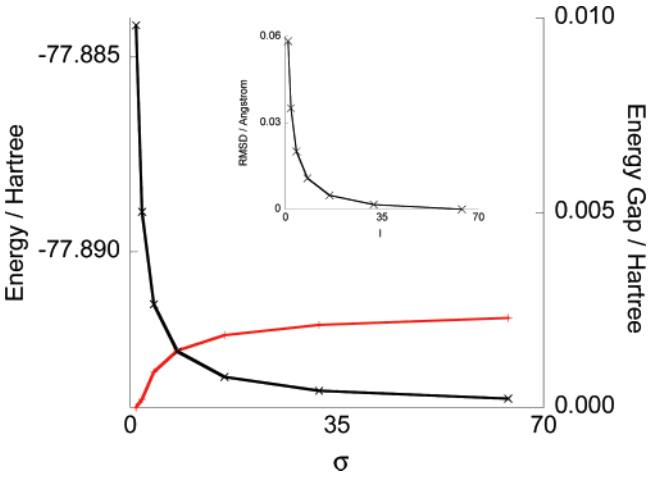

Figure 3. Convergence behavior as a function of σ for MECI optimizations of the twisted-pyramidalized intersection of ethylene. The smoothing parameter, α, is held constant at 0.02 Hartree for all optimizations. The total energy (red) and energy gap (black) are shown. The rms deviation relative to the converged ($\sigma = 64$) MECI geometry is shown in the inset.

subject to the constraint that the energy gap separating states I and J vanishes. In Yarkony's method,[42] the Lagrange multipliers are fully optimized. In contrast, the Bearpark−Robb−Schlegel method[17] applies the constraints with a fixed multiplier and projected gradients to simplify implementation. In both cases, the energy difference gradient and derivative coupling ($\vec{g}$ and $\vec{h}$, respectively) vectors are required. These vectors are defined as

$$(\vec{g}_{IJ})_i = \frac{\partial}{\partial R_i}(\langle\psi_1|\hat{H}|\psi_I\rangle - \langle\psi_J|\hat{H}|\psi_J\rangle) \equiv \frac{\partial}{\partial R_i}(E_I - E_J) \quad (1)$$

$$(\vec{h}_{IJ})_i = (E_J - E_I)\left\langle\psi_I\left|\frac{\partial\psi_J}{\partial R_i}\right.\right\rangle \quad (2)$$

The $\vec{g}$ and $\vec{h}$ vectors span the "branching plane" comprised of the molecular displacements that lift the degeneracy in first order in the neighborhood of a conical intersection connecting two adiabatic electronic states. The energies of the Ith and Jth adiabatic electronic states exhibit derivative discontinuities for displacements along the branching plane directions at a conical intersection. When three or more electronic states conically intersect, the branching space becomes higher than two-dimensional, and additional displacement vectors can be defined which lift the degeneracy in first order and specify the directions along which derivative discontinuities of the adiabatic energies are expected.[43,44]

As discussed above, we desired a method which could optimize MECI geometries without knowledge of the derivative coupling vector. Traditional optimization methods assume smoothness of the function being minimized. This is problematic in the case of MECI optimization because the derivatives of both upper and lower PESs exhibit discontinuities for geometries along the intersection seam. Knowledge of $\vec{g}$ and $\vec{h}$ allows one to avoid exploration in directions where the function is nonsmooth and this is the reason that the Yarkony and BRS methods require these vectors. The MECI optimization method described here is a variant of the sequential penalty method[45] and requires only energy information. If energy gradients are available, these can be used directly and the method will be more efficient. Thus, this scheme can be applied in conjunction with any quantum chemical method capable of describing multiple electronic states, regardless of whether derivative couplings (or even analytic gradients) are readily available.

TABLE 1: Energies (in eV) of MECIs for Ethylene and Formaldiminium Calculated Using CAS, MS-CASPT2, and MRSDCI Methods[a]

	CAS		MS-CASPT2		MRSDCI	
	S_0	S_1	S_0	S_1	S_0	S_1
Ethylene						
Franck−Condon Pt	0.00	10.27	0.00	8.67	0.00	9.33
twist-pyr	5.62	5.65	4.81	4.82	5.11	5.14
ethylidene	4.47	4.49	4.71	4.73	4.75	4.76
Formaldiminium						
Franck−Condon Pt	0.00	8.81	0.00	7.85	0.00	8.24
twisted	3.63	3.64	3.25	3.26	3.40	3.43
methylimine	4.82	4.82	5.30	5.31	5.23	5.24

[a] The zero of energy corresponds to the Franck−Condon point for the respective level of theory.

In order to find an intersection between states I and J (where $I = J + 1$), we seek a minimum of the objective function

$$F_{IJ}(\vec{R}; \sigma, \alpha) = \bar{E}_{IJ}(\vec{R}) + \sigma G_{IJ}(\Delta E_{IJ}(\vec{R});\alpha) \quad (3)$$

where

$$\bar{E}_{IJ}(\vec{R}) = \frac{E_I(\vec{R}) + E_J(\vec{R})}{2} \quad (4)$$

and

$$\Delta E_{IJ}(\vec{R}) = E_I(\vec{R}) - E_J(\vec{R}) \quad (5)$$

The penalty function $G_{IJ}(\Delta E_{IJ}(\vec{R});\alpha)$ is a monotonically increasing function of the energy gap, defined in eq 5 such that it is always positive, and $\vec{R}$ is the vector of molecular coordinates. The parameters σ and α are user defined constants, discussed in more detail below. Essentially, minimization of eq 3 corresponds to minimizing the average energy of states I and J subject to the constraint that the gap between the states vanishes. The penalty function should (1) vanish when the energy gap vanishes, (2) tend toward the energy gap when the energy gap is large, and (3) remain differentiable at all geometries. A simple form which satisfies these requirements is

$$G_{IJ}(\Delta E_{IJ}; \alpha) = \frac{\Delta E_{IJ}^{\,2}}{\Delta E_{IJ} + \alpha} \quad (6)$$

where α can be recognized as a smoothing parameter. As can be shown by application of the chain rule, the penalty function of eq 6 remains differentiable at a conical intersection even though the derivative of the energy gap is discontinuous (as long as α is nonzero and the derivative of the energy gap is finite, which will always be the case for realistic conical intersections). Our use of $\bar{E}_{IJ}(\vec{R})$ and a penalty function which is differentiable in the region around the intersection is similar in spirit to the extrapolatable functions used by Yarkony.[18] If analytic derivatives of the energy are available the gradient of $F_{IJ}(\vec{R};\lambda,\alpha)$ can be readily calculated

$$\frac{dF_{IJ}(\vec{R};\sigma,\alpha)}{d\vec{R}} = \frac{1}{2}\left(\frac{dE_I(\vec{R})}{d\vec{R}} + \frac{dE_J(\vec{R})}{d\vec{R}}\right) + \sigma\frac{\Delta E_{IJ}^{\,2} + 2\alpha\Delta E_{IJ}}{(\Delta E_{IJ} + \alpha)^2}\left(\frac{dE_I(\vec{R})}{d\vec{R}} - \frac{dE_J(\vec{R})}{d\vec{R}}\right) \quad (7)$$

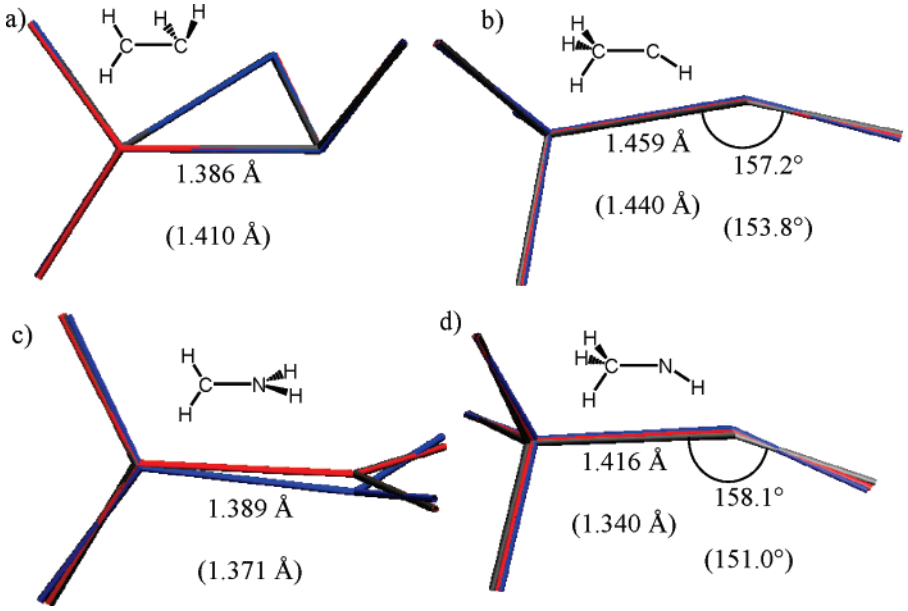

Figure 4. Optimized geometries for the MECIs of ethylene (a and b) and formaldiminium (c and d). Geometries at several levels of theory are superimposed for each intersection: CAS (gray), MS-CASPT2 (blue), and MRSDCI (red). Selected geometric parameters are shown for CAS, MS-CASPT2 (in parenthesis) and MRSDCI (in brackets). The ethylene twisted-pyramidalized and ethylidene MECIs are shown in a and b, respectively. The formaldiminium twisted and methylamine MECIs are shown in c and d, respectively. There is qualitative agreement of the geometries at the various levels of theory in a, b, and d. In the formaldiminium twisted MECI (c) the MS-CASPT geometry is significantly pyramidalized about the nitrogen atom, while the CAS and MRSDCI geometries are not.

For finite σ, the minimum $F_{IJ}(\vec{R};\sigma,\alpha)$ is not a true MECI. At the optimized geometry, $\vec{R}_{\text{opt}}(\sigma,\alpha)$, where the gradient of F_{IJ} vanishes, one can show that (see Supporting Information)

$$\Delta E_{IJ}(\vec{R}_{\text{opt}}(\sigma,\alpha)) = \alpha\left(\sqrt{\frac{\sigma Z}{1+\sigma Z}} - 1\right) \tag{8}$$

where

$$Z = \left.\frac{\nabla\Delta E_{IJ}\cdot\nabla\bar{E}_{IJ}}{\nabla\bar{E}_{IJ}\cdot\nabla\bar{E}_{IJ}}\right|_{\vec{R}=\vec{R}_{\text{opt}}(\sigma,\alpha)} \tag{9}$$

In the limits where σ goes to infinity or α goes to zero, $\Delta E(\vec{R}_{\text{opt}})$ will vanish and $\vec{R}_{\text{opt}}$ is the MECI geometry. Figure 1 illustrates this behavior. Unfortunately, in either of these limits $d^2F_{IJ}(\vec{R})/d\vec{R}^2$ and $d^3F_{IJ}(\vec{R})/d\vec{R}^3$ approach infinity near $\vec{R}_{\text{opt}}(\sigma,\alpha)$, and therefore optimization becomes intractable.

In practice, we set a threshold δ corresponding to the maximum acceptable gap for a conical intersection ($\delta = 0.001$ Hartree in this work). We choose initial values for α and σ (usually 0.02 Hartree and 3.5 respectively) and minimize F_{IJ}. If the resulting gap between the states exceeds δ, we increase σ and repeat the optimization. The parameter σ is increased repeatedly until $\Delta E_{IJ}(\vec{R}_{\text{opt}}(\sigma,\alpha)) \leq \delta$. At this point, we are satisfied that $\vec{R}_{\text{opt}}(\sigma,\alpha)$ is an MECI.

The energy gap at the final optimized geometry will always be finite but arbitrarily small. Thus, one might wonder whether the optimized geometry truly corresponds to a conical intersection or whether it is instead a weakly avoided crossing. Other numerical conical intersection optimization schemes generally share this slight ambiguity; the only way to ensure that a particular geometry corresponds to a conical intersection is to calculate the electronic wavefunction along a loop encircling the intersection and show that it changes sign.[46] Even this procedure is not foolproof since Renner−Teller intersections are not accompanied by Berry's phase.[47] However, in practice, it is usually not necessary to demonstrate that a geometry corresponds to a true intersection, conical or otherwise. First, it is the presence of a near-zero gap which dominates the observed nonadiabatic effects. Second, it has been argued that it is almost always the case that a geometry with small energy gap is located close to a true intersection.[48]

In principle, any minimization algorithm may be used in the above procedure. We have successfully implemented and used Powell's conjugate direction method, conjugate gradient, and the Broyden−Fletcher−Goldfarb−Shannon (BFGS) quasi-Newton scheme.[49] We use the BFGS scheme for most of the results presented here. We demand that three criteria are met simultaneously for convergence to be achieved at a given value of σ

$$F_{IJ}(\vec{R}_{\text{prior}};\sigma,\alpha) - F_{IJ}(\vec{R};\sigma,\alpha) \leq tol_{\text{step}} \tag{10}$$

$$\frac{1}{\sigma}\frac{dF_{IJ}(\vec{R};\sigma,\alpha)}{d\vec{R}}\cdot\vec{u} \leq tol_{\text{grad}} \tag{11}$$

$$\left|\frac{dF_{IJ}(\vec{R};\sigma,\alpha)}{d\vec{R}} - \left(\frac{dF_{IJ}(\vec{R};\sigma,\alpha)}{d\vec{R}}\cdot\vec{u}\right)\vec{u}\right| \leq tol_{\text{grad}} \tag{12}$$

where $\vec{u}$ is a unit vector directed along the penalty

$$\vec{u} = \frac{\dfrac{dG_{IJ}(\vec{R};\alpha)}{d\vec{R}}}{\left|\dfrac{dG_{IJ}(\vec{R};\alpha)}{d\vec{R}}\right|} \tag{13}$$

The first criteria demands that the size of the last step taken by the optimizer be small. The second and third criteria consider the gradient of $F_{IJ}(\vec{R};\sigma,\alpha)$. It is separated into two components: parallel and perpendicular to $dG_{IJ}(\vec{R};\alpha)/d\vec{R}$. Both components must be lower than a threshold, but a stricter criteria is applied to the perpendicular gradient. This ensures that optimization within the seam space is not compromised if σ becomes large. Typical values for tol_{step} and tol_{grad} are 10^{-6} Hartree and 0.005 Hartree/Bohr, respectively.

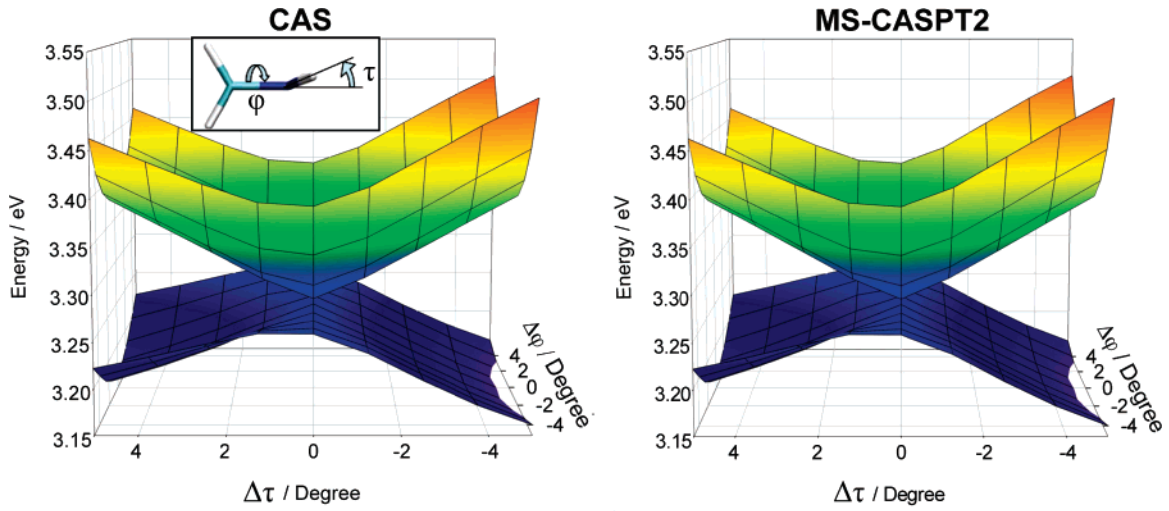

Figure 5. Potential energy surfaces in the vicinity of the formaldiminium twisted S_1/S_0 MECI, optimized at the CAS and MS-CASPT2 levels of theory. Pyramidalization and torsional angles (shown in the inset) are expressed as deviations from the MECI geometry. Despite a significant difference in geometry between the CAS and MS-CASPT2 MECIs (see Figure 4), the topography of the surrounding PES is essentially the same.

TABLE 2: Energies (in eV) of MECIs for Larger Molecules Calculated Using CAS and MS-CASPT2 Methods[a]

	CAS				MS-CASPT2			
	S_0	S_1	S_2	S_3	S_0	S_1	S_2	S_3
Butadiene								
Franck−Condon Pt	0.00	6.69	8.51	11.21	0.00	6.50	6.73	8.78
S_1/S_0 methylene+	6.02	6.04	8.95	11.21	4.00	4.01	7.24	8.30
S_1/S_0 methylene-	5.39	5.40	8.72	12.50	4.34	4.36	7.59	10.09
S_1/S_0 transoid	5.25	5.26	9.56	10.50	4.44	4.46	7.92	8.71
S_2/S_1	3.13	6.35	6.37	8.79	2.74	5.33	5.33	6.31
$S_3/S_2/S_1$ 3-state	3.51	7.13	7.18	7.23	2.69	5.57	5.59	5.62
Stilbene								
Franck−Condon Pt	0.00	5.95	10.74		0.00	5.73	8.27	
S_1/S_0 twist-pyr	4.81	4.82	9.46		4.05	4.05	8.60	
S_1 minimum	2.98	4.78	6.89		4.05	4.05	8.60	
GFP Chromophore Anion								
Franck−Condon Pt	0.00	4.15			0.00	3.16		
S_1/S_0	3.04	3.05			2.56	2.55		
S_1 minimum	1.60	2.77			0.83	2.14		

[a] The zero of energy is the Franck−Condon point at the respective level of theory.

The location of minimal energy three state intersections (ME3CIs) is achieved by optimizing the objective function

$$F_{IJK}(\vec{R};\sigma,\alpha) = F_{IJ}(\vec{R};\sigma,\alpha) + F_{IK}(\vec{R};\sigma,\alpha) + F_{JK}(\vec{R};\sigma,\alpha) \quad (14)$$

where $I = J + 1$ and $I = K + 2$. $F_{IJK}(\vec{R};\sigma,\alpha)$ is differentiable at intersections between any pair of states I, J, and K and the simultaneous intersection of the three. In practice, we find that a somewhat larger value of σ (e.g., 10) is necessary relative to the two state case for acceptable convergence rates.

In a dynamical system, the MECI may or may not be the point on the intersection seam which is most likely to be accessed. To further explore the intersection seam, our method has been expanded to allow the location of the intersection point which is closest to (minimally distant from) a reference geometry (e.g., the intersection point which is nearest the excited-state minimum or nearest the Franck−Condon point). Optimization of these minimal distance conical intersections (MDCIs) can be used to explore the nature of the intersection seam above and beyond the MECI.

The MDCI optimization scheme is similar to the MECI optimization scheme. The total objective function for MDCI searches takes the form

$$F_{IJ,\mathrm{MDCI}}(\vec{R};\sigma,\alpha,\alpha_{\mathrm{MW}}) = \frac{D_{\mathrm{MW}}{}^2}{D_{\mathrm{MW}} + \alpha_{\mathrm{MW}}} + \sigma G_{IJ}(\Delta E(\vec{R});\alpha) \quad (15)$$

where α_{MW} is a second empirical smoothing parameter. The mass weighted distance, D_{MW}, is defined as

$$D_{\mathrm{MW}} = \sqrt{\sum_{\eta=1}^{N_{\mathrm{coord}}} m_\eta (R_\eta - R_{\eta,\mathrm{ref}})^2} \quad (16)$$

where N_{coord} is the total number of nuclear degrees of freedom (indexed by η), m_η is the mass associated with the ηth degree of freedom, and $R_{\eta,\mathrm{ref}}$ is the ηth element of the reference geometry. We have found that $\alpha_{\mathrm{MW}} = 0.1$ Å and an initial value for the penalty multiplier of

$$\sigma = 6\sqrt{\sum_{\eta=1}^{N_{\mathrm{coord}}} m_\eta} \quad (17)$$

work well.

It would be possible to replace the first term of $F_{IJ,\mathrm{MDCI}}(\vec{R};\sigma,\alpha,\alpha_{\mathrm{MW}})$ with $D_{\mathrm{MW}}{}^2$ with similar results. However, the slope of $D_{\mathrm{MW}}{}^2$ becomes arbitrarily large as $\vec{R}$ gets farther from $\vec{R}_{\mathrm{ref}}$, and thus, a larger value of σ is required to achieve a constraint force large enough to enforce the constraint on the energy gap. Our choice of the first term of $F_{IJ,\mathrm{MDCI}}(\vec{R};\sigma,\alpha,\alpha_{\mathrm{MW}})$ has a slope which is bounded for large values of $|\vec{R} - \vec{R}_{\mathrm{ref}}|$. Thus, the appropriate value of σ does not depend so strongly on $\vec{R}$.

Conceptually, $F_{IJ,\mathrm{MDCI}}(\vec{R};\sigma,\alpha,\alpha_{\mathrm{MW}})$ is very similar to $F_{IJ}(\vec{R};\sigma,\alpha)$. Instead of minimizing $E_{IJ}(\vec{R})$ subject to the constraint that $\Delta E(\vec{R}_{\mathrm{opt}})$ is zero, D_{MW} is minimized subject to the same constraint. Because D_{MW} is not differentiable at the reference geometry a smoothed function of D_{MW} is used, similar to the smoothed gap function, $G_{IJ}(\Delta E_{IJ}(\vec{R});\alpha)$.

This method has been implemented in the Conical Intersection Optimizer (CIOpt) software package. CIOpt is available for free download from the Materials Computation Center Software

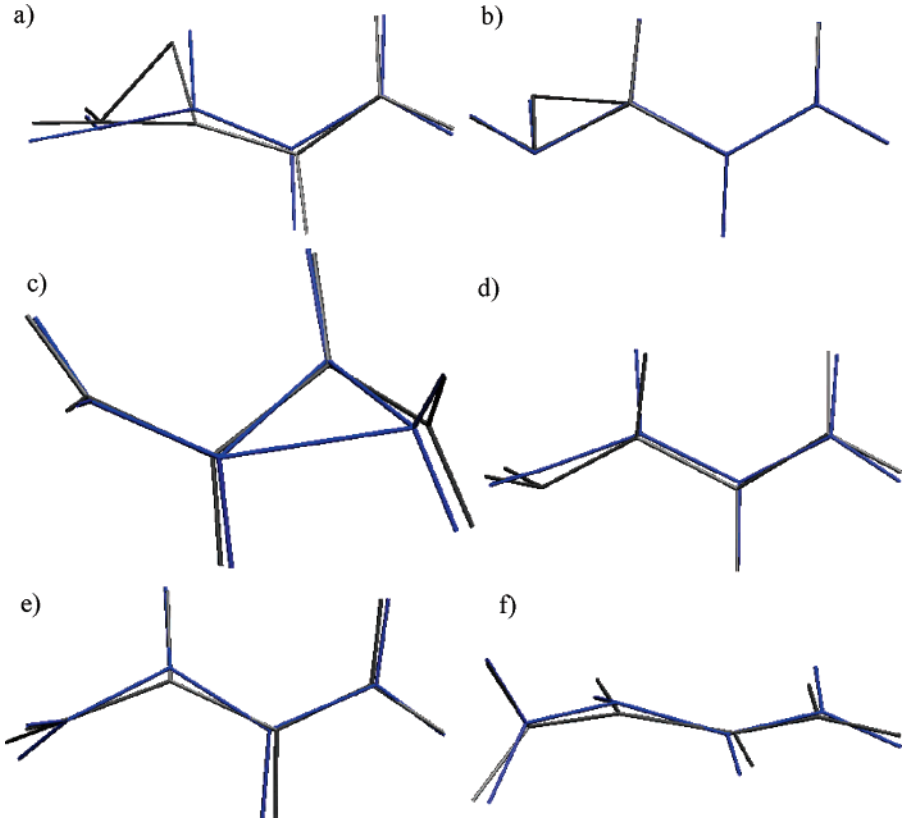

Figure 6. Optimized geometries for MECIs of butadiene. Geometries at the CAS (gray) and MS-CASPT2 (blue) levels of theory are superimposed. The Me^+, Me^-, and transoid S_1/S_0 intersections are shown in panels a−c. The S_2/S_1 MECI is shown in panel d. Two different views of the $S_3/S_2/S_1$ ME3CI are shown in panels e and f. Qualitative agreement of the geometries can be seen for the S_1/S_0 MECIs, though there are significant quantitative differences for the Me^+ S_1/S_0 MECI. CAS predicts a greater degree of pyramidalization about the twisted terminal carbon in the S_2/S_1 MECI compared to MS-CASPT2. For the ME3CI, MS-CASPT2 predicts a greater degree of pyramidalization about the carbon adjacent to the twisted methylene group than does CAS.

Archive (http://www.mcc.uiuc.edu/software/). It is designed to be easily interfaced with any electronic structure code via a template-based scheme. CIOpt can be used with any electronic structure method capable of calculating energies for multiple electronic states.

Results and Discussion

All electronic structure calculations were carried out with the MolPro suite.[50] Analytic gradients of the MS-CASPT2 energy are used where possible.[51] Although analytic gradients for MRSDCI have been implemented,[52] they are not yet available in the MolPro suite. Thus, the MRSDCI optimizations described below were performed without the benefit of analytic gradients. When the state-averaged CAS method is used, the parameters will be abbreviated in the form SA-*N*-CAS(*m*/*n*) where *N* is the number of singlet states included in the state average, *m* is the number of active electrons, and *n* is the number of active orbitals. The parameters of the reference space for MS-CASPT2 and MRSDCI will also be abbreviated this way. The 6-31G** basis[53,54] is used in all calculations unless otherwise noted. Similarly, all valence orbitals are correlated in all MS-CASPT2 and MRSDCI calculations unless stated otherwise.

We carried out conical intersection optimizations for a variety of molecules in order to characterize our optimization scheme and to assess the differences between intersections optimized with CAS, MS-CASPT2, and MRSDCI. The left panel of Figure 2 shows the convergence behavior of $\bar{E}_{IJ}$ and ΔE_{IJ} for a typical optimization. The algorithm first locates a point near the conical intersection seam; that is, ΔE_{IJ} drops dramatically in the first few iterations. In subsequent iterations, the optimization follows the seam while lowering $\bar{E}_{IJ}$. At iteration 28, convergence is achieved. However, $\Delta E_{IJ} > \delta$; thus, σ is increased and the optimization continues. Only four more iterations are required to achieve convergence with the new value of σ, and ΔE_{IJ} is now less than δ. The right panel of Figure 2 shows the same data from a typical optimization using the Bearpark−Robb−Schlegel algorithm as implemented in the MolPro electronic structure software package. Convergence is achieved after a similar number of iterations.

We have also investigated the convergence behavior with respect to σ. Figure 3 shows converged values of $\bar{E}_{IJ}$, ΔE_{IJ}, and the root mean squared deviations of each converged geometry for a typical set of simulations with different initial values of σ. All three of these quantities converge smoothly as σ is increased.

A series of optimizations were performed with decreasing values of δ to demonstrate how the computational cost of the algorithm depends on the maximum allowed energy gap. Decreasing δ from 0.001 to 0.0001 Hartree results in a need for 22 additional iterations to converge. Decreasing it from 0.0001 to 0.00001 Hartree requires 13 additional iterations, and from 0.00001 to 0.000001 Hartree requires 14 more iterations. Thus, it is preferable to choose as large a value of δ as is acceptable.

Several MECIs connecting the S_0 and S_1 electronic states have been optimized for ethylene[55] and its protonated Schiff base analogue, formaldiminium, at the CASSCF, MS-CASPT2, and MRSDCI levels of theory. In all cases, the underlying multi-

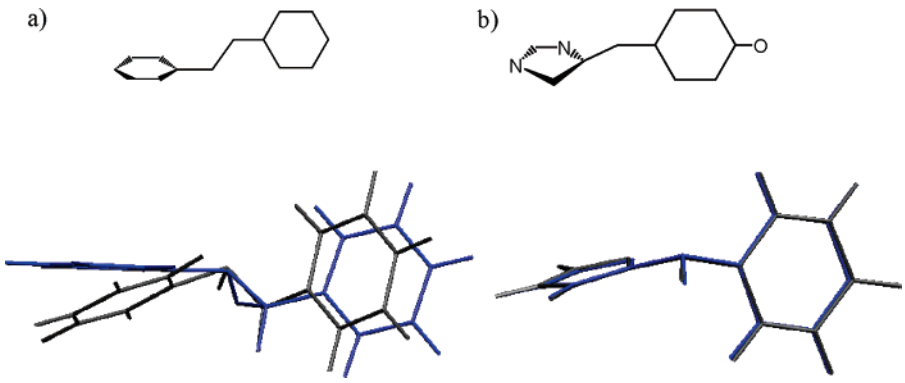

Figure 7. Optimized S_1/S_0 MECI geometries for (a) stilbene and (b) GFP chromophore anion. Geometries at the CAS (gray) and MS-CASPT2 (blue) levels of theory are superimposed. Qualitative agreement of the geometries at the two levels of theory can be seen in both cases. For stilbene, the MS-CASPT2 S_1/S_0 MECI geometry exhibits more hydrogen migration character than the CAS MECI geometry.

reference wavefunction corresponds to SA-2-CAS(2/2). The MECI geometries are compared in Figure 4. The differences between the geometries for three of the four MECIs are negligible, with the only discernible difference being in the case of the twisted formaldiminium MECI (Figure 4c). In this case, the CASSCF and MRSDCI geometries are purely twisted, whereas the CASPT2 geometry is slightly pyramidalized. This may be an indication that the intersection seam is relatively flat with respect to pyramidalization.

The MECI energies (relative to the Franck−Condon point for each molecule) are given in Table 1. The differences in the energetics are more pronounced than the differences in MECI geometries, largely because the vertical excitation energies are strongly affected by dynamic electron correlation. However, there are also significant differences in the relative energies of different MECIs in the same molecule at the different levels of theory. For example, the ethylidene and twisted-pyramidalized MECIs in ethylene are nearly degenerate in MS-CASPT2 but much less so in CASSCF. It is notable that, in both energetics and geometric parameters listed in Figure 4, the MRSDCI values fall between those predicted by CAS and MS-CASPT2. The potential energy surface in the vicinity of the twisted formaldiminium MECIs at the CAS and MS-CASPT2 levels of theory are plotted in Figure 5. Despite a significant change in the MECI geometries, the topography of the intersections is unchanged: both have a similar "peaked" shape.[56]

We also optimized MECIs at the CAS and MS-CASPT2 levels of theory in butadiene, stilbene, and the anionic form of the green fluorescent protein (GFP) chromophore. Energetic information for these molecules is collected in Table 2.

Comparisons of the resulting MECI geometries for butadiene using SA-4-CAS(4/4) and SA-4-CAS(4/4)-MSPT2 are shown in Figure 6. Three distinct S_1/S_0 MECIs have been located. Two of these (Figure 6a,b) involve charge transfer states, and the third (Figure 6c) involves only covalent states. The two MECIs involving charge-transfer character differ according to whether the twisted terminal methylene group is positively (Me^+) or negatively (Me^-) charged. Interestingly, as shown in Table 2, the relative energies of the charge transfer and covalent intersections are reversed at the MS-CASPT2 level of theory relative to CAS. The covalent (transoid) MECI is the lowest energy S_0/S_1 MECI at the CAS level of theory, but it is the highest energy S_0/S_1 MECI when MS-CASPT2 is used. This should not be surprising since dynamic electron correlation effects are largest for ionic states, and CASSCF methods are well-known to artificially destabilize ionic states. As seen in Figure 6a−c, the geometries of the three S_1/S_0 MECIs optimized at the CAS and MS-CASPT2 levels of theory are in qualitative agreement.

Since S_2 is the optically accessed state in *trans*-butadiene at the chosen levels of theory, it is also interesting to locate an S_2/S_1 MECI geometry. We have found such an MECI, shown in Figure 6d. This S_2/S_1 MECI exhibits considerably more pyramidalization about the twisted terminal carbon using CASSCF compared to MS-CASPT2.

Finally, we have also located an $S_3/S_2/S_1$ ME3CI for butadiene, shown in Figure 6e,f. The ME3CI is below the S_2 energy at the Franck−Condon point in both CAS and MS-CASPT2, indicating that it might play a role in the photochemistry of *trans*-butadiene. This is an interesting case of three-state intersections because the molecule would likely approach the intersection on S_2, on the middle state of the ME3CI. Dynamics calculations would be very interesting to elucidate this behavior. Relatively minor differences between the geometries of the ME3CI at the CAS and MS-CASPT2 levels of theory are seen in Figure 6e,f. Slight pyramidalization about one of the central carbons is observed with MS-CASPT2, but this is absent when CAS is used. This difference and the previously noted pyramidalization in the S_2/S_1 MECI may be related to the unbalanced treatment of charge transfer states due to the neglect of dynamic electron correlation in CAS.

For stilbene, two geometries known to be important to the photochemistry include a twisted-pyramidalized S_1/S_0 MECI and a twisted S_1 minimum.[57] We optimized these geometries using SA-3-CAS(2/2) and SA-3-CAS(2/2)-MSPT2. In order to decrease the computational effort, we left 36 orbitals uncorrelated in the MS-CASPT2 calculation. Some possibly very significant changes were seen between CAS and MS-CASPT2 at these levels of theory. At the CAS level, the S_1/S_0 MECI is somewhat above (<0.1 eV) the S_1 minimum. However, MS-CASPT2 finds the S_1/S_0 MECI to be the absolute minimum on the S_1 surface. This might imply a large difference in the excited-state lifetimes which would be predicted by CAS and MS-CASPT2, although dynamics simulations would be needed to make this more concrete. Figure 7a shows the S_0/S_1 MECI geometries obtained with CAS and MS-CASPT2. They are qualitatively similar in that they are both twisted and pyramidalized with some hydrogen migration character. However, the degree of hydrogen migration is higher at the MS-CASPT2 level of theory.

The S_1/S_0 MECI and the nearby S_1 minimum were optimized for the GFP chromophore anion[14] using SA-2-CAS(2/2) and SA-2-CAS(2/2)-MSPT2. Again, due to computational expense, we left 36 orbitals uncorrelated in the MS-CASPT2 calculations. Both the MECI geometries and energetics are in good agree-

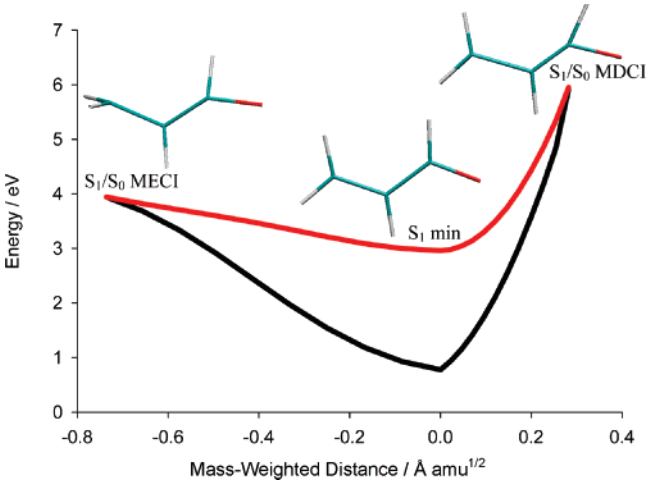

Figure 8. S_0 (black) and S_1 (red) energies (relative to the S_0 minimum) of a path (linearly interpolated in internal coordinates) connecting three important geometries on the potential energy surface of acrolein. The S_1 minimum, S_1/S_0 MECI, and the point on the S_1/S_0 CI seam which is closest in mass-weighted distance to the S_1 minimum (MDCI) are shown. All three geometries are optimized at the SA3-CAS(6/5)/6-31G* level of theory. The vertical excitation energy to the bright S_2 state is 7.55 eV, thus all points shown here are energetically accessible after optical excitation to the lowest bright excited state. The S_1/S_0 MECI is twisted about the C−C double bond and slightly pyramidalized about the terminal carbon, unlike the S_1 minimum geometry, which is planar. The S_1/S_0 MDCI is planar with a compressed ∠OCH and lies 2 eV above the S_1/S_0 MECI. Only a dynamical simulation could determine which of the MECI or MDCI geometries dominates quenching.

ment. Both CAS and MS-CASPT2 predict that there is a well-defined S_1 minimum lying below the S_1/S_0 MECI. The S_0/S_1 MECI geometry is twisted and pyramidalized in both CAS and MS-CASPT2, as depicted in Figure 7b.

To illustrate the optimization of MDCIs, the S_1/S_0 conical intersection nearest the S_1 minimum in acrolein was optimized using SA-3-CAS(6/5) and the 6-31G* basis set. A slice of the ground and excited state PESs along a set of geometries connecting this MDCI, the S_1 minimum, and the S_1/S_0 MECI is shown in Figure 8. Notice that the S_1/S_0 MECI in acrolein[58] is of a "sloped" topography,[56] while most of the MECIs we have optimized in this paper have been of the "peaked" variety. We did not encounter any difficulty optimizing this MECI, suggesting that the performance of our new algorithm is not affected significantly by the topography of the MECI. The MDCI is 2.0 eV above the MECI, which might lead one to believe it will not be important in the dynamics. However, the optically bright state is S_2 and the vertical excitation energy is 6.41 and 7.55 eV from experiment or SA-3-CAS(6/5), respectively. Thus, the molecule clearly has enough energy to access the MDCI after excitation to S_2. The path from the minimum to each intersection is barrierless, but the MDCI is much closer to the minimum than the MECI. The MDCI and S_1 minimum geometries are both planar, differing primarily in the degree of hydrogen migration character. The MECI geometry is qualitatively different from the other two, involving twisting about the C−C double bond and slight pyramidalization about the terminal carbon. Only an accurate dynamical simulation could determine which region of the intersection seam will be accessed more often, the region around the MECI or that near the MDCI. The utility of these MDCI geometries remains to be seen by comparison to dynamics simulations, but it is safe to say that knowing such geometries could give a more complete understanding of possible decay paths and the structure of the intersection space.

Conclusions

We have reported the first complete optimization of minimal energy conical intersections at the MS-CASPT2 level of theory. We developed a novel MECI optimization scheme which does not require derivative coupling vectors. This scheme is based on a smoothed objective function which is differentiable at intersection points. It can easily be applied with any electronic structure method capable of calculating multiple electronic states.

This scheme is implemented in the CIOpt software package. CIOpt can easily be interfaced with any electronic structure package via a template-based interface and is freely available. A future version of CIOpt will allow geometric constraints to be applied. This feature can be used to trace out a seam of intersections, so that the more global nature of the intersection seam can be considered.

Utilizing analytic gradients of the MS-CASPT2 surface we optimized MECIs in molecules as large as stilbene and GFP chromophore. The multistate (and not the single state) variant of CASPT2 must be used to describe the topography around conical intersections correctly, specifically to obtain the correct dimensionality of the branching space which lifts the degeneracy. CIOpt has also been employed without analytic gradients to optimize MRSDCI MECIs for ethylene and formaldiminium.

This method extends naturally to allow the optimization of three state intersections. A minimal energy three state conical intersection was reported for 1,3-butadiene at the CAS and MS-CASPT2 levels of theory. This intersection is below the vertical excitation energy at both levels of theory and may play a role in the dynamics.

This method was also extended to optimize MDCIs, conical intersection points nearest in mass-weighted Cartesian coordinates to a reference geometry. The optimization of MDCIs was illustrated for the acrolein molecule where the nearest intersection to the S_1 minimum is found. Only dynamical simulations can determine their relative importance, but we hope that MDCIs may become a useful tool in mapping out the structure of the intersection spaces of molecules.

In most but not all cases, there is qualitative agreement between the geometries of the MECIs optimized at the CAS, MS-CASPT2, and MRSDCI geometries. The most notable exception is the twisted intersection in formaldiminium which is purely twisted at the CAS and MRSDCI levels of theory but pyramidalized about the nitrogen at the MS-CASPT2 level.

Greater differences emerge between methods if the energetics are considered. As expected, the vertical excitation energies are much lower in MS-CASPT2 than in CAS. However, there are also disagreements concerning relative energies of MECIs in some cases. For example, in butadiene, the relative energies of the three S_1/S_0 MECIs we located are reversed at the MS-CASPT2 level of theory relative to CAS. Large changes in the relative energies of intersections are also observed in ethylene and formaldiminium. In stilbene, the twisted-pyramidalized intersection is slightly above the S_1 minimum at the CAS level of theory but becomes the absolute S_1 minimum at the MS-CASPT2 level of theory. Future work should investigate the extent to which these differences persist when larger active spaces are used.

In general MRSDCI and MS-CASPT2 are in better agreement than MS-CASPT2 and CAS. A pattern emerges when all three methods are considered: The MRSDCI value (whether it be a

relative energy or a geometric parameter) is often bounded by the CAS and MS-CASPT2 values.

This new methodology allows more accurate characterization of conical intersections in molecules. The availability of more accurate geometries and energies of MECIs could be useful in estimating rates of nonadiabatic transitions. In addition, this new tool can be used to help assess the accuracy of PESs calculated with lower cost electronic structure methods, for example CAS surfaces used in first principles dynamical simulations.

Acknowledgment. This work was supported by NSF (DMR-03-25939 and CHE-02-311876) with additional support through the Frederick Seitz Materials Research Laboratory (DOE DEFG02-91ER45439) at the University of Illinois. B.G.L. is a Lubrizol Fellow.

Supporting Information Available: Cartesian coordinates for all geometries discussed in the text, energies for relevant electronic states, and detailed derivation of eq 8 from eq 7. This material is available free of charge via the Internet at http://pubs.acs.org.

References and Notes

(1) Robb, M. A.; Olivucci, M. *J. Photochem. Photobiol.* **2001**, *144A*, 237.
(2) Yarkony, D. R. *Acc. Chem. Res.* **1998**, *31*, 511.
(3) Levine, B. G.; Martinez, T. J. *Ann. Rev. Phys. Chem.* **2007**, *58*, 613.
(4) Martinez, T. J. *Acc. Chem. Res.* **2006**, *39*, 119.
(5) Yarkony, D. R. *J. Chem. Phys.* **2001**, *114*, 2601.
(6) Yarkony, D. R. *J. Phys. Chem.* **2001**, *105A*, 6277.
(7) Ben-Nun, M.; Molnar, F.; Schulten, K.; Martínez, T. J. *Proc. Natl. Acad. Sci.* **2002**, *99*, 1769.
(8) Robb, M. A.; Bernardi, F.; Olivucci, M. *Pure Appl. Chem.* **1995**, *67*, 783.
(9) Ruiz, D. S.; Cembran, A.; Garavelli, M.; Olivucci, M.; Fuss, W. *Photochem. Photobiol.* **2002**, *76*, 622.
(10) Coto, P. B.; Sinicropi, A.; De Vico, L.; Ferre, N.; Olivucci, M. *Mol. Phys.* **2006**, *104*, 983.
(11) Coe, J.; Martinez, T. J. *J. Am. Chem. Soc.* **2005**, *127*, 4560.
(12) Crespo-Hernandez, C. E.; Cohen, B.; Hare, P. M.; Kohler, B. *Chem. Rev.* **2004**, *104*, 1977.
(13) Migani, A.; Robb, M. A.; Olivucci, M. *J. Am. Chem. Soc.* **2003**, *125*, 2804.
(14) Toniolo, A.; Ben-Nun, M.; Martínez, T. J. *J. Phys. Chem. A* **2002**, *106*, 4679.
(15) Toniolo, A.; Thompson, A. L.; Martinez, T. J. *Chem. Phys.* **2004**, *304*, 133.
(16) Celani, P.; Bernardi, F.; Olivucci, M.; Robb, M. A. *J. Chem. Phys.* **1995**, *102*, 5733.
(17) Bearpark, M. J.; Robb, M. A.; Schlegel, H. B. *Chem. Phys. Lett.* **1994**, *223*, 269.
(18) Yarkony, D. R. *J. Phys. Chem. A* **2004**, *108*, 3200.
(19) Zilberg, S.; Haas, Y. *Chem. Eur. J.* **1999**, *5*, 1755.
(20) Koga, N.; Morokuma, K. *Chem. Phys. Lett.* **1985**, *119*.
(21) Saxe, P.; Lengsfield, B. H.; Yarkony, D. R. *Chem. Phys. Lett.* **1985**, *113*, 159.
(22) Roos, B. O. *Adv. Chem. Phys.* **1987**, *69*, 399.
(23) Dallos, M.; Lischka, H.; Shepard, R.; Yarkony, D. R.; Szalay, P. G. *J. Chem. Phys.* **2004**, *120*, 7330.
(24) Lischka, H.; Dallos, M.; Szalay, P. G.; Yarkony, D. R.; Shepard, R. *J. Chem. Phys.* **2004**, *120*, 7322.
(25) Petersilka, M.; Gossmann, U. J.; Gross, E. K. U. *Phys. Rev. Lett.* **1996**, *76*, 1212.
(26) Piecuch, P.; Kowalski, K.; Pimienta, I. S. O.; Fan, P. D.; Lodriguito, M.; McGuire, M. J.; Kucharski, S. A.; Kus, T.; Musial, M. *Theor. Chem. Acc.* **2004**, *112*, 349.
(27) Toniolo, A.; Granucci, G.; Martinez, T. J. *J. Phys. Chem. A* **2003**, *107*, 3822.
(28) Spezia, R.; Burghardt, I.; Hynes, J. T. *Mol. Phys.* **2006**, *104*, 903.
(29) Burghardt, I.; Cederbaum, L. S.; Hynes, J. T. *Faraday Discuss.* **2004**, *127*, 395.
(30) Burghardt, I.; Hynes, J. T. *J. Phys. Chem.* **2006**, *110A*, 11411.
(31) Toniolo, A.; Olsen, S.; Manohar, L.; Martinez, T. J. *Faraday Discuss.* **2004**, *127*, 149.
(32) Toniolo, A.; Olsen, S.; Manohar, L.; Martinez, T. J. Ultrafast Excited State Dynamics in Green Fluorescent Protein Chromophore. In *Ultrafast Molecular Events in Chemistry and Biology: Femtochemistry VI*; Martin, M., Hynes, J. T., Eds.; Elsevier: Amsterdam, 2004.
(33) Yamazaki, S.; Kato, S. *J. Chem. Phys.* **2005**, *123*, 114510.
(34) Yamazaki, S.; Kato, S. *J. Am. Chem. Soc.* **2007**, *129*, 2901.
(35) Migani, A.; Sinicropi, A.; Ferre, N.; Cembran, A.; Garavelli, M.; Olivucci, M. *Faraday Discuss.* **2004**, *127*, 179.
(36) Levine, B. G.; Ko, C.; Quenneville, J.; Martinez, T. J. *Mol. Phys.* **2006**, *104*, 1053.
(37) Roos, B. O. *Acc. Chem. Res.* **1999**, *32*, 137.
(38) Andersson, K.; Malmqvist, P.-A.; Roos, B. O.; Sadlej, A. J.; Wolinski, K. *J. Phys. Chem.* **1990**, *94*, 5483.
(39) Finley, J.; Malmqvist, P.-A.; Roos, B. O.; Serrano-Andres, L. *Chem. Phys. Lett.* **1998**, *288*, 299.
(40) Serrano-Andres, L.; Merchan, M. *J. Chem. Phys.* **2005**, *122*, 104107.
(41) Page, C. S.; Olivucci, M. *J. Comp. Chem.* **2003**, *24*, 298.
(42) Manaa, M. R.; Yarkony, D. R. *J. Chem. Phys.* **1993**, *99*, 5251.
(43) Matsika, S.; Yarkony, D. R. *J. Chem. Phys.* **2002**, *117*, 6907.
(44) Matsika, S.; Yarkony, D. R. *J. Am. Chem. Soc.* **2003**, *125*, 10672.
(45) Fletcher, R. *Practical Methods of Optimization*; John Wiley and Sons: New York, 1987.
(46) Xantheas, S. S.; Atchity, G. J.; Elbert, S. T.; Ruedenberg, K. *J. Chem. Phys.* **1991**, *94*, 8054.
(47) Yarkony, D. R. *Rev. Mod. Phys.* **1996**, *68*, 985.
(48) Truhlar, D. G.; Mead, C. A. *Phys. Rev. A* **2003**, *68*, 032501.
(49) Press, W. H.; Teukolsky, S. A.; Vetterling, W. T.; Flannery, B. P. *Numerical Recipes in FORTRAN*; Cambridge Press: Cambridge, U.K., 1992.
(50) MOLPRO, version 2006.1, a package of ab initio programs, H.-J. Werner, P. J. Knowles, R. Lindh, F. R. Manby, M. Schutz, P. Celani, T. Korona, G. Rauhut, R. D. Amos, A. Bernhardsson, A. Berning, D. L. Cooper, M. J. O. Deegan, A. J. Dobbyn, F. Eckert, C. Hampel, and G. Hetzer, A. W. Lloyd, S. J. McNicholas, W. Meyer and M. E. Mura, A. Nicklass, P. Palmieri, U. Schumann, H. Stoll, A. J. Stone, R. Tarroni, and T. Thosteinsson.
(51) Celani, P.; Werner, H.-J. *J. Chem. Phys.* **2003**, *119*, 5044.
(52) Shepard, R.; Lischka, H.; Szalay, P. G.; Kovar, T.; Ernzerhof, M. *J. Chem. Phys.* **1992**, *96*, 2085.
(53) Frisch, M. J.; Pople, J. A.; Binkley, J. S. *J. Chem. Phys.* **1984**, *80*, 3265.
(54) Hehre, W. J.; Ditchfield, R.; Pople, J. A. *J. Chem. Phys.* **1972**, *56*, 2257.
(55) Ben-Nun, M.; Martínez, T. J. *Chem. Phys.* **2000**, *259*, 237.
(56) Atchity, G. J.; Xantheas, S. S.; Ruedenberg, K. *J. Chem. Phys.* **1991**, *95*, 1862.
(57) Quenneville, J.; Martínez, T. J. *J. Phys. Chem. A* **2003**, *107*, 829.
(58) Lee, A. M. D.; Coe, J. D.; Ullrich, S.; Ho, M.-L.; Lee, S.-J.; Cheng, B.-M.; Zgierski, M. Z.; Chen, I.-C.; Martinez, T. J.; Stolow, A. *J. Phys. Chem. A* **2007**, in press.